Incorporating knowledge on the measurement noise in electrical impedance tomography

M. Dambrine, H. Harbrecht and B. Puig

Departement Mathematik und Informatik
Fachbereich Mathematik
Universität Basel
CH-4051 Basel

Preprint No. 2017-14
October 2017

www.math.unibas.ch

INCORPORATING KNOWLEDGE ON THE MEASUREMENT NOISE IN ELECTRICAL IMPEDANCE TOMOGRAPHY

MARC DAMBRINE, HELMUT HARBRECHT, AND BENEDICTE PUIG

Abstract. The present article is concerned with the identification of an obstacle or void of different conductivity which is included in a two-dimensional domain by measurements of voltage and currents at the boundary. In general, the voltage distribution is prescribed and hence deterministic. Whereas, the current distribution is measured and contains measurement errors. We assume that some information is given on these measurement errors which can be described by means of a random field. We exploit this extra knowledge by minimizing a linear combination of the expectation and the variance of the Kohn-Vogelius functional. It is shown how these ideas can be realized in numerical computations. By numerical results, the applicability and feasibility of our approach is demonstrated.

Introduction

Electrical impedance tomography is used in medical imaging to reconstruct the electric conductivity of a part of the body from measurements of currents and voltages at the surface [23]. The same technique is also used in geophysical explorations. An important special case consists in reconstructing the shape of an unknown inclusion or void assuming (piecewise) constant conductivities. In this case, only one pair of current/voltage measurements is necessary, in principle.

The problem under consideration is a special case of the general conductivity reconstruction problem and is severely ill-posed. It has been intensively investigated as an inverse problem. We refer for example to [1, 4, 9, 21] for numerical algorithms and to [5, 17] for particular results concerning uniqueness. Moreover, we refer to [7, 8] for methods using the full Dirichlet-to-Neumann map at the outer boundary.

In [29], the problem under consideration has been reformulated as a shape optimization problem for the Kohn-Vogelius functional (see [26]). Then, seeking the unknown inclusion is equivalent to seeking the minimizer of an energy functional. Much attention has been spent on the analysis of this approach ([2, 3, 13]) and its comparison with a least-squares tracking type functionals. It is also sufficiently versatile to be used in the context of fluid mechanics [6].

HH has been supported by the Swiss National Science Foundation through the project $\mathcal{H}$-*matrix based first and second moment analysis.*

Our objective in this article is to take advantage of properties of the noise to construct a deterministic formulation which incorporates this knowledge. We assume that the measured flux is given as a random field that models the measurement errors. We then aim at minimizing a combination of the expectation and the variance of the Kohn-Vogelius functional. As we will show, both quantities can easily be computed via deterministic quantities. The associated shape gradients can likewise be deterministically computed.

The rest of this article is organized as follows. In Section 1, we present the physical model and reformulate the identification problem as shape optimization problem. We introduce the random model and compute the expectation and the variance of the shape functional and their shape gradients. As we will see, both are given by deterministic expressions under some structure assumptions on the random fields under consideration. Then, Section 2 is concerned with the discretization of the shape optimization problem. We assume that the sought inclusion is a starshaped domain which enables us to approximate it by a finite Fourier series. The state equations are reformulated as boundary integral equations which are discretized by means of a fast wavelet boundary element method of linear complexity. In Section 3, we present numerical results which validate the feasibility of the present approach. Finally, in Section 4, we state concluding remarks.

1. Problem formulation

1.1. **Physical model.** Let $T \in \mathbb{R}^d$, $d = 2, 3$, be a simply connected domain with boundary $\Sigma = \partial T$ and assume that an unknown simply connected inclusion S with regular boundary $\Gamma = \partial S$ is located inside the domain T satisfying $\operatorname{dist}(\Sigma, \Gamma) > 0$, cf. Figure 1.1. In order to determine the inclusion S, we measure the current distribution $g \in H^{-1/2}(\Sigma)$ at the boundary Σ for a given voltage distribution $f \in H^{1/2}(\Sigma)$. Hence, we are seeking a domain $D := T \setminus \overline{S}$ and an associated harmonic function u, satisfying the system of equations

$$\begin{aligned} \Delta u &= 0 && \text{in } D, \\ u &= 0 && \text{on } \Gamma, \\ u = f,\ \frac{\partial u}{\partial \mathbf{n}} &= g && \text{on } \Sigma. \end{aligned} \tag{1.1}$$

This system is an overdetermined boundary value problem which admits a solution only for the true inclusion S. In accordance with e.g. [25], the inclusion's boundary Γ is uniquely determined from $f \neq 0$ and g. Nonetheless, it is well known that the problem of finding the inclusion's boundary Γ is severely ill-posed. Especially, the measured data g contain noise.

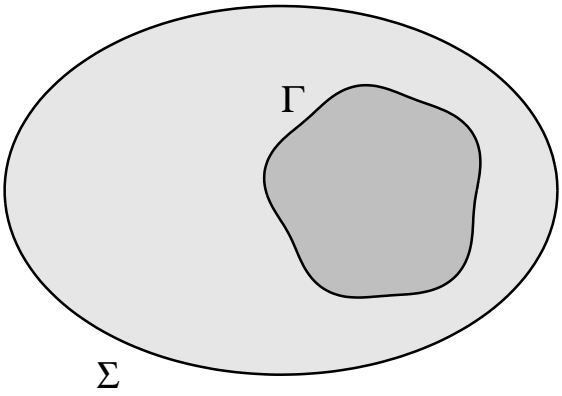

FIGURE 1.1. The domain D and its boundaries Γ and Σ.

1.2. **Formulation as shape optimization problem.** Following [29], we introduce the auxiliary harmonic functions v and w, satisfying

$$\begin{aligned} \Delta v = 0 \qquad \Delta w = 0 \qquad & \text{in } D, \\ v = 0 \qquad w = 0 \qquad & \text{on } \Gamma, \\ \frac{\partial v}{\partial \mathbf{n}} = g \qquad w = f \qquad & \text{on } \Sigma, \end{aligned}$$

and consider the following shape optimization problem

$$J(D) = \int_D \|\nabla(v-w)\|^2 \,\mathrm{d}\mathbf{x} = \int_\Sigma \left(g - \frac{\partial w}{\partial \mathbf{n}}\right)(v-f)\,\mathrm{d}\sigma \to \inf. \tag{1.2}$$

Herein, the infimum has to be taken over all domains which have a void with sufficiently regular boundary. We refer to [29] for the existence of optimal solutions with respect to this shape optimization problem.

The shape gradient to (1.2) has also been computed in [29]. For variation fields $\mathbf{V} : \mathbb{R}^d \to \mathbb{R}$, being sufficiently smooth, it holds that

$$\delta J(D)[\mathbf{V}] = \int_\Gamma \langle \mathbf{V}, \mathbf{n}\rangle \left[\left(\frac{\partial v}{\partial \mathbf{n}}\right)^2 - \left(\frac{\partial w}{\partial \mathbf{n}}\right)^2\right] \mathrm{d}\sigma. \tag{1.3}$$

see also [29]. Given an inclusion Σ such the overdetermined boundary problem (1.1) has a solution, the necessary first order optimality condition $\delta J(D)[\mathbf{V}] = 0$ is satisfied for all admissible variations $\mathbf{V}$. Notice that the shape Hessian for (1.2) has been computed and analyzed in [13].

1.3. **Random model.** We shall now assume that we have some extra knowledge on the errors which are caused by the measurement of g. Then, we can model g as a random field. To that end, let $(\Omega, \mathcal{S}, \mathbb{P})$ be a complete probability space and assume that $g : \Sigma \times \Omega \to \mathbb{R}$ is a random field which belongs to the Bochner space $L^2_{\mathbb{P}}(\Omega, H^{-1/2}(\Sigma))$.

Let us recall for the reader's convenience the definition of Bochner spaces. Consider a real number $p \geq 1$. Then, for a Banach space X, the Bochner space $L^p_{\mathbb{P}}(\Omega, X)$ consists of all functions $v : \Omega \to X$ whose norm

$$\|v\|_{L^p_{\mathbb{P}}(\Omega,X)} := \begin{cases} \left(\int_\Omega \|v(\cdot,\omega)\|_X^p \, \mathrm{d}\mathbb{P}(\omega) \right)^{1/p}, & p < \infty, \\ \operatorname*{ess\,sup}_{\omega\in\Omega} \|v(\cdot,\omega)\|_X, & p = \infty, \end{cases}$$

is finite. If $p = 2$ and X is a Hilbert space, then the Bochner space is isomorphic to the tensor product space $L^2_{\mathbb{P}}(\Omega) \otimes X$.

Since the data $L^2_{\mathbb{P}}(\Omega, H^{-1/2}(\Sigma))$ are random, also the state v will be a random field. It satisfies $v \in L^2_{\mathbb{P}}(\Omega, H^1(\Omega))$ by linearity of the underlying partial differential equation. As a consequence, the shape functional J become also a random process.

Two strategies are *a priori* available to deal with such a random shape functional. The first one consist in minimizing each realization of the objective and then taking an average of the minimizers. This strategy has been presented in the context of Bernoulli's free boundary problem in [11]. Nonetheless, this approach is unrealistic here due to its high computational cost.

We therefore propose in this article to address the second approach. Namely, we minimize an averaged shape functional as considered in [10]. In particular, we will minimize a combination of the expectation and the variance of the shape functional (1.2). In other words, we seek the domain D with inclusion S such that either

$$F(D) = (1-\alpha)\mathbb{E}\big[J(D,\omega)\big] + \alpha\mathbb{V}\big[J(D,\omega)\big] \to \inf \tag{1.4}$$

or even

$$F(D) = (1-\alpha)\mathbb{E}\big[J(D,\omega)\big] + \alpha\sqrt{\mathbb{V}\big[J(D,\omega)\big]} \to \inf, \tag{1.5}$$

where the random shape functional reads as

$$J(D,\omega) = \int_D \big\|\nabla\big(v(\omega) - w\big)\big\|^2 \, \mathrm{d}\mathbf{x} \to \inf \tag{1.6}$$

and the states read as

$$\begin{aligned} \Delta v(\omega) &= 0 & \Delta w &= 0 & &\text{in } D, \\ v(\omega) &= 0 & w &= 0 & &\text{on } \Gamma, \\ \frac{\partial v}{\partial \mathbf{n}}(\omega) &= g(\omega) & w &= f & &\text{on } \Sigma. \end{aligned} \tag{1.7}$$

Let us explain the meaning of the averaged objective defined in (1.4) and (1.5), respectively. When the weight α is equal to 0, we consider only the average value of the Kohn-Vogelius functional. Its minimization means to be good on a regular base, but does not prohibit a flat

distribution and, hence, being often with high values of the of the objective. In order to obtain a shape around which the distribution of the objective is more narrow, we can penalize the variance of the Kohn-Vogelius functional by increasing the weight α. Notice that the standard deviation in scales like the expectation which makes (1.5) better suited to achieve this goal in comparison with (1.4). The range of admissible α is $[0, 1)$, since the expectation is neglected when $\alpha = 1$. Then, only the reduction of variance matters and not the average value at all, losing all interest in the shape identification.

Concerning the existence of an optimal shape for the minimization of the objective defined in (1.4) or (1.5), the situation is the same than for the original problem: minimizing J. In the class of open subsets of T, we do not have an existence result. Existence holds once the class of admissible domains is restricted to some class of domains for which one obtains compactness and the continuity of the solution of the Dirichlet problem with respect to the shape (compare [22]): the class of domains with a uniform exterior cone property for example.

For what follows, we should make the assumption that the Neumann data g are given by the expansion

$$g(\mathbf{x}, \omega) = g_0(\mathbf{x}) + \sum_{i=1}^{M} g_i(\mathbf{x}) Y_i(\omega), \tag{1.8}$$

where the random variable $Y_i(\omega)$ are independent and identically distributed random variables, $Y_i \sim Y$, being centered, $\mathbb{E}[Y] = 0$, normalized, $\mathbb{V}[Y] = 1$, and having finite fourth order moments. Thus, there especially hold the identities

$$\mathbb{E}[g(\omega)] = g_0 \quad \text{and} \quad \mathbb{V}[g(\omega)] = \sum_{i=1}^{M} g_i^2.$$

Note that we have in mind several independent measurements of the current distribution for the same voltage distribution, from which we can derive the sample mean and the sample covariance. Then, assuming that $g(\mathbf{x}, \omega)$ is a Gaussian random field, the expansion (1.8) can be derived from by means of the Karhunen-Loève expansion, see [18, 27] for example.

Given the expansion (1.8), the linearity of the state equation (1.7) implies that

$$v(\mathbf{x}, \omega) = v_0(\mathbf{x}) + \sum_{i=1}^{M} v_i(\mathbf{x}) Y_i(\omega), \tag{1.9}$$

where v_i solves the equation

$$\Delta v_i = 0 \text{ in } D, \quad v_i = 0 \text{ on } \Gamma, \quad \frac{\partial v_i}{\partial \mathbf{n}} = g_i \text{ on } \Sigma. \tag{1.10}$$

In particular, if g is a Gaussian random field, then also v is a Gaussian random field.

1.4. **Expectation and variance of the random shape functional.** We shall show that the expectation and the variance of the random shape functional (1.6) can be computed from deterministic quantities.

Proposition 1.1. *It holds*

$$\mathbb{E}\big[J(D,\omega)\big] = \sum_{i=1}^{M} \int_\Sigma v_i g_i \,\mathrm{d}\sigma + \int_\Sigma \left(g_0 - \frac{\partial w}{\partial \mathbf{n}} \right) (v_0 - f) \,\mathrm{d}\sigma. \tag{1.11}$$

Proof. Following the ideas from [10], using Fubini's theorem for non negative functions, the expectation of the random shape functional can be rewritten as

$$\begin{aligned}
\mathbb{E}\big[J(D,\omega)\big] &= \int_\Omega \int_D \big\| \nabla\big(v(\omega) - w\big) \big\|^2 \,\mathrm{d}\mathbf{x} \,\mathrm{d}\mathbb{P}(\omega) \\
&= \int_D \int_\Omega \big\| \nabla\big(v(\omega) - w\big) \big\|^2 \,\mathrm{d}\mathbb{P}(\omega) \,\mathrm{d}\mathbf{x} \\
&= \int_D \left[\int_\Omega \big\langle \nabla\big(v(\mathbf{x},\omega) - w(\mathbf{x})\big), \nabla\big(v(\mathbf{y},\omega) - w(\mathbf{y})\big) \big\rangle \,\mathrm{d}\mathbb{P}(\omega) \right]\Bigg|_{\mathbf{x}=\mathbf{y}} \mathrm{d}\mathbf{x}.
\end{aligned}$$

In view of the expansion (1.9), we thus conclude

$$\begin{aligned}
\mathbb{E}\big[J(D,\omega)\big] = \int_D \Bigg[\int_\Omega \Bigg\langle \nabla\Bigg(v_0(\mathbf{x}) + \sum_{i=1}^{M} v_i(\mathbf{x}) Y_i(\omega) - w(\mathbf{x}) \Bigg), \\
\nabla\Bigg(v_0(\mathbf{y}) + \sum_{j=1}^{M} v_j(\mathbf{y}) Y_j(\omega) - w(\mathbf{y}) \Bigg) \Bigg\rangle \,\mathrm{d}\mathbb{P}(\omega) \Bigg]\Bigg|_{\mathbf{x}=\mathbf{y}} \mathrm{d}\mathbf{x}.
\end{aligned}$$

Making now use of the fact that $Y_i \sim Y$ are independent and identically distributed random variables, we arrive at

$$\begin{aligned}
\mathbb{E}\big[J(D,\omega)\big] &= \int_D \Bigg[\sum_{i,j=1}^{M} \langle \nabla v_i(\mathbf{x}), \nabla v_j(\mathbf{y}) \rangle \mathbb{E}[Y_i Y_j] - 2 \sum_{i=1}^{M} \langle \nabla v_i(\mathbf{x}), \nabla\big(v_0(\mathbf{y}) - w(\mathbf{y})\big) \rangle \mathbb{E}[Y_i] \\
&\qquad + \langle \nabla\big(v_0(\mathbf{x}) - w(\mathbf{x})\big), \nabla\big(v_0(\mathbf{x}) - w(\mathbf{y})\big) \rangle \Bigg]\Bigg|_{\mathbf{x}=\mathbf{y}} \mathrm{d}\mathbf{x} \\
&= \int_D \Bigg[\sum_{i=1}^{M} \|\nabla v_i(\mathbf{x})\|^2 \mathbb{E}[Y^2] - 2 \sum_{i=1}^{M} \langle \nabla v_i(\mathbf{x}), \nabla\big(v_0(\mathbf{x}) - w(\mathbf{x})\big) \rangle \mathbb{E}[Y] \\
&\qquad + \big\| \nabla\big(v_0(\mathbf{x}) - w(\mathbf{x})\big) \big\|^2 \Bigg] \mathrm{d}\mathbf{x}.
\end{aligned}$$

Finally, we can exploit that Y is centered and normalized to arrive at

$$\mathbb{E}\big[J(D,\omega)\big] = \int_D \left[\sum_{i=1}^{M} \|\nabla v_i(\mathbf{x})\|^2 + \big\| \nabla\big(v_0(\mathbf{x}) - w(\mathbf{x})\big) \big\|^2 \right] \mathrm{d}\mathbf{x}.$$

Integration by parts and observing $\partial v_i/\partial \mathbf{n} = g_i$ in accordance with (1.10) yields thus (1.11). $\square$

In complete analogy, one can derive a deterministic expression for the variance of the random shape functional.

Proposition 1.2. *It holds*

$$\begin{aligned}\mathbb{V}\big[J(D,\omega)\big] = (\mathbb{E}[Y^4]-3)\sum_{i=1}^{M}\bigg(\int_\Sigma v_i g_i \,\mathrm{d}\sigma\bigg)^2 \\ - 4\mathbb{E}[Y^3]\sum_{i=1}^{M}\bigg(\int_\Sigma v_i g_i \,\mathrm{d}\sigma\bigg)\bigg(\int_\Sigma g_i(v_0-f)\,\mathrm{d}\sigma\bigg) \\ + 2\sum_{i,j=1}^{M}\bigg(\int_\Sigma v_i g_j \,\mathrm{d}\sigma\bigg)^2 + 4\sum_{i=1}^{M}\bigg(\int_\Sigma g_i(v_0-f)\,\mathrm{d}\sigma\bigg)^2.\end{aligned} \tag{1.12}$$

Proof. Due to the knowledge of (1.11), the variance can be computed from the uncentered second moment of the shape functional in accordance with

$$\mathbb{V}\big[J(D,\omega)\big] = \mathbb{E}\big[J(D,\omega)^2\big] - \mathbb{E}^2\big[J(D,\omega)\big].$$

The starting point to derive the uncentered second moment is

$$\begin{aligned}\mathbb{E}\big[J(D,\omega)^2\big] &= \int_\Omega \bigg[\int_D \big\|\nabla\big(v(\omega)-w\big)\big\|^2 \,\mathrm{d}\mathbf{x}\bigg]^2 \,\mathrm{d}\mathbb{P}(\omega) \\ &= \int_D\int_D\int_\Omega \big\|\nabla\big(v(\mathbf{x},\omega)-w(\mathbf{x})\big)\big\|^2\big\|\nabla\big(v(\mathbf{y},\omega)-w(\mathbf{y})\big)\big\|^2 \,\mathrm{d}\mathbb{P}(\omega)\,\mathrm{d}\mathbf{y}\,\mathrm{d}\mathbf{x}.\end{aligned}$$

By inserting again the expansion (1.9) of the random field v and straightforward calculation, we obtain

$$\begin{aligned}
\mathbb{E}\big[J(D,\omega)^2\big] = \int_D \int_D \Bigg[& \sum_{i,j,k,\ell=1}^{M} \langle \nabla v_i(\mathbf{x}), \nabla v_j(\mathbf{x})\rangle \langle \nabla v_k(\mathbf{y}), \nabla v_\ell(\mathbf{y})\rangle \mathbb{E}[Y_i Y_j Y_k Y_\ell] \\
& - 4 \sum_{i,j,k=1}^{M} \langle \nabla v_i(\mathbf{x}), \nabla v_j(\mathbf{x})\rangle \langle \nabla v_k(\mathbf{y}), \nabla \big(v_0(\mathbf{y}) - w(\mathbf{y})\big)\rangle \mathbb{E}[Y_i Y_j Y_k] \\
& + \sum_{i,j=1}^{M} \Big\{ 2 \langle \nabla v_i(\mathbf{x}), \nabla v_j(\mathbf{x})\rangle \big\| \nabla \big(v_0(\mathbf{y}) - w(\mathbf{y})\big)\big\|^2 \\
& \qquad + 4 \langle \nabla v_i(\mathbf{x}), \nabla \big(v_0(\mathbf{x}) - w(\mathbf{x})\big)\rangle \langle \nabla v_j(\mathbf{y}), \nabla \big(v_0(\mathbf{y}) - w(\mathbf{y})\big)\rangle \Big\} \mathbb{E}[Y_i Y_j] \\
& - 4 \sum_{i=1}^{M} \langle \nabla v_i(\mathbf{x}), \nabla \big(v_0(\mathbf{x}) - w(\mathbf{x})\big)\rangle \big\| \nabla \big(v_0(\mathbf{y}) - w(\mathbf{y})\big)\big\|^2 \mathbb{E}[Y_i] \\
& \qquad + \big\| \nabla \big(v_0(\mathbf{x}) - w(\mathbf{x})\big)\big\|^2 \big\| \nabla \big(v_0(\mathbf{y}) - w(\mathbf{y})\big)\big\|^2 \Bigg] \, \mathrm{d}\mathbf{y} \, \mathrm{d}\mathbf{x}.
\end{aligned}$$

Of course, this deterministic expression can further be simplified by using the independence of the random variable $Y_i \sim Y$. Namely, in view of $\mathbb{E}[Y] = 0$ and $\mathbb{V}[Y] = 1$, it holds

$$\begin{aligned}
\mathbb{E}\big[J(D,\omega)^2\big] = \mathbb{E}^2\big[J(D,\omega)\big] & + (\mathbb{E}[Y^4] - 3) \sum_{i=1}^{M} \bigg(\int_D \|\nabla v_i(\mathbf{x})\|^2 \, \mathrm{d}\mathbf{x} \bigg)^2 \\
& - 4\mathbb{E}[Y^3] \sum_{i=1}^{M} \bigg(\int_D \|\nabla v_i(\mathbf{x})\|^2 \, \mathrm{d}\mathbf{x} \bigg) \bigg(\int_D \langle \nabla v_i(\mathbf{y}), \nabla \big(v_0(\mathbf{y}) - w(\mathbf{y})\big)\rangle \, \mathrm{d}\mathbf{x} \bigg) \\
& + 2 \sum_{i,j=1}^{M} \bigg(\int_D \langle \nabla v_i(\mathbf{x}), \nabla v_j(\mathbf{x})\rangle \, \mathrm{d}\mathbf{x} \bigg)^2 \\
& + 4 \sum_{i=1}^{M} \bigg(\int_D \langle \nabla v_i(\mathbf{x}), \nabla \big(v_0(\mathbf{x}) - w(\mathbf{x})\big)\rangle \, \mathrm{d}\mathbf{x} \bigg)^2.
\end{aligned}$$

Finally, integration by parts yields the desired expression (1.12). □

We have a further simplification of (1.12) in the most important situation of Gaussian random fields.

Corollary 1.3. *If g is a Gaussian random field, then*

$$\mathbb{V}\big[J(D,\omega)\big] = 2 \sum_{i,j=1}^{M} \bigg(\int_\Sigma v_i g_j \, \mathrm{d}\sigma \bigg)^2 + 4 \sum_{i=1}^{M} \bigg(\int_\Sigma g_i (v_0 - f) \, \mathrm{d}\sigma \bigg)^2. \tag{1.13}$$

Proof. In the case of a Gaussian random field, the random variables obey the normal law, i.e., $Y \sim \mathcal{N}(0,1)$. By injecting that it thus holds $\mathbb{E}[Y^4] = 3$ and $\mathbb{E}[Y^3] = 0$, we derive the assertion immediately from (1.12). □

This is the expression we will exploit in our numerical examples. Especially, for sake of convenience, we will provide the shape gradient only for the specific formula (1.13) in the next subsection and not for the general case (1.12).

1.5. **Shape gradient of the expectation and of the variance.** We shall compute next the shape gradient of the expectation and of the variance. For a survey on the shape calculus, we refer the reader to [12, 28, 30] and the references therein.

Obviously, due to linearity, the shape gradient $\delta\big(\mathbb{E}\big[J(D,\omega)\big]\big)[\mathbf{V}]$ of the shape functional $\mathbb{E}[J(D,\omega)]$ into the direction of the perturbation field $\mathbf{V}$ is just given by $\mathbb{E}\big[\delta J(D,\omega)[\mathbf{V}]\big]$. Hence, it is computed according to

$$\begin{aligned}\delta\big(\mathbb{E}\big[J(D,\omega)\big]\big)[\mathbf{V}] &= \mathbb{E}\big[\delta J(D,\omega)[\mathbf{V}]\big] \\ &= \int_\Omega \int_\Gamma \langle \mathbf{V}, \mathbf{n}\rangle \left[\left(\frac{\partial v}{\partial \mathbf{n}}(\omega)\right)^2 - \left(\frac{\partial w}{\partial \mathbf{n}}\right)^2\right] \mathrm{d}\sigma \,\mathrm{d}\mathbb{P}(\omega) \\ &= \int_\Gamma \langle \mathbf{V}, \mathbf{n}\rangle \left\{ \left[\int_\Omega \frac{\partial v}{\partial \mathbf{n}}(\mathbf{x},\omega) \frac{\partial v}{\partial \mathbf{n}}(\mathbf{y},\omega) \,\mathrm{d}\mathbb{P}(\omega)\right]\Big|_{\mathbf{x}=\mathbf{y}} - \left(\frac{\partial w}{\partial \mathbf{n}}(\mathbf{x})\right)^2 \right\} \mathrm{d}\sigma.\end{aligned}$$

We insert the expansion (1.9) and exploit again that the random variables $Y_i \sim Y$ are independent, identically distributed, centered and normalized to arrive at the final expression:

$$\delta\big(\mathbb{E}\big[J(D,\omega)\big]\big)[\mathbf{V}] = \int_\Gamma \langle \mathbf{V}, \mathbf{n}\rangle \left[\sum_{i=0}^{M} \left(\frac{\partial v_i}{\partial \mathbf{n}}\right)^2 - \left(\frac{\partial w}{\partial \mathbf{n}}\right)^2\right] \mathrm{d}\sigma.$$

Of course, we could alternatively have computed the shape derivative of the deterministic shape functional (1.11), yielding the same result.

In case of the variance of the random shape functional (1.6), the situation becomes somewhat more difficult. It can be derived by using directly the derivative of the shape functional's second uncentered moment:

$$\delta\big(\mathbb{E}\big[J(D,\omega)\big]\big)[\mathbf{V}] = \delta\bigg(\int_\Omega J^2(D,\omega)\,\mathrm{d}\mathbb{P}(\omega)\bigg)[\mathbf{V}] = 2\int_\Omega J(D,\omega)\delta J(D,\omega)[\mathbf{V}]\,\mathrm{d}\mathbb{P}(\omega).$$

However, since we are mainly interested in Gaussian random fields $g(\mathbf{x},\omega)$, i.e., $Y_i \sim \mathcal{N}(0,1)$ in (1.8) and (1.9), respectively, we will provide only the shape derivative of (1.13).

Proposition 1.4. *Assume that it holds $Y_i \sim \mathcal{N}(0,1)$ in (1.8). Then, we have*

$$\delta\big(\mathbb{V}\big[J(D,\omega)\big]\big)[\mathbf{V}] = 4\sum_{i,j=1}^{M}\bigg(\int_\Sigma v_i g_j \,\mathrm{d}\sigma\bigg)\bigg(\int_\Gamma \langle \mathbf{V},\mathbf{n}\rangle \frac{\partial v_i}{\partial \mathbf{n}}\frac{\partial v_j}{\partial \mathbf{n}}\,\mathrm{d}\sigma\bigg) + 8\sum_{i=1}^{M}\bigg(\int_\Sigma g_i(v_0-f)\,\mathrm{d}\sigma\bigg)\bigg(\int_\Gamma \langle \mathbf{V},\mathbf{n}\rangle \frac{\partial v_i}{\partial \mathbf{n}}\frac{\partial v_0}{\partial \mathbf{n}}\,\mathrm{d}\sigma\bigg).$$

Proof. Since only the functions v_i's depend on the domain D, the shape derivative of (1.13) reads

$$\delta\big(\mathbb{V}\big[J(D,\omega)\big]\big)[\mathbf{V}] = 4\sum_{i,j=1}^{M}\bigg(\int_\Sigma v_i g_j \,\mathrm{d}\sigma\bigg)\bigg(\int_\Sigma \delta v_i g_j \,\mathrm{d}\sigma\bigg) + 8\sum_{i=1}^{M}\bigg(\int_\Sigma g_i(v_0-f)\,\mathrm{d}\sigma\bigg)\bigg(\int_\Sigma g_i \delta v_0 \,\mathrm{d}\sigma\bigg), \tag{1.14}$$

where the local shape derivatives $\delta v_i = \delta v_i[\mathbf{V}]$ satisfy the boundary value problems

$$\Delta \delta v_i = 0 \text{ in } D, \quad \delta v_i = -\langle \mathbf{V},\mathbf{n}\rangle \frac{\partial v_i}{\partial \mathbf{n}} \text{ on } \Gamma, \quad \frac{\partial v_i}{\partial \mathbf{n}} = 0 \text{ on } \Sigma. \tag{1.15}$$

Using that $\partial v_i/\partial \mathbf{n} = g_i$, we obtain for all $i,j = 0,1,\ldots,M$ by integration by parts

$$\int_\Sigma \delta v_i g_j \,\mathrm{d}\sigma + \int_\Gamma \delta v_i \frac{\partial v_j}{\partial \mathbf{n}}\,\mathrm{d}\sigma = \int_\Sigma \underbrace{\frac{\partial \delta v_i}{\partial \mathbf{n}}}_{=0} v_j \,\mathrm{d}\sigma + \int_\Gamma \frac{\partial \delta v_i}{\partial \mathbf{n}} \underbrace{v_j}_{=0}\,\mathrm{d}\sigma = 0.$$

This, in view of (1.15), means that

$$\int_\Sigma \delta v_i g_j \,\mathrm{d}\sigma = \int_\Gamma \langle \mathbf{V},\mathbf{n}\rangle \frac{\partial v_i}{\partial \mathbf{n}}\frac{\partial v_j}{\partial \mathbf{n}}\,\mathrm{d}\sigma$$

for all $i,j = 0,1,\ldots,M$. By inserting the latter identities into (1.14), we arrive at the desired assertion. □

We mention that the shape derivative of the standard deviation is given by the chain rule in accordance with

$$\delta\sqrt{\mathbb{V}\big[J(D,\omega)\big]}[\mathbf{V}] = \frac{\delta\big(\mathbb{V}\big[J(D,\omega)\big]\big)[\mathbf{V}]}{2\sqrt{\mathbb{V}\big[J(D,\omega)\big]}}.$$

2. Numerical realization

Since the numerical realization is based on the adaptation of the classical Kohn-Vogelius approach for electrical impedance tomography, we briefly recall the ingredients and refer to [13, 14] for more details.

2.1. **Boundary integral equations.** We will compute the unknown boundary data of the state functions v and w by boundary integral equations. We introduce the single layer and the double layer operator with respect the boundaries $\Phi, \Psi \in \{\Gamma, \Sigma\}$ by

$$(V_{\Phi\Psi}u)(\mathbf{x}) := -\frac{1}{2\pi}\int_\Phi \log\|\mathbf{x}-\mathbf{y}\|u(\mathbf{y})\,\mathrm{d}\sigma_{\mathbf{y}}, \qquad \mathbf{x}\in\Psi,$$
$$(K_{\Phi\Psi}u)(\mathbf{x}) := \frac{1}{2\pi}\int_\Phi \frac{\langle \mathbf{x}-\mathbf{y}, \mathbf{n}_{\mathbf{y}}\rangle}{\|\mathbf{x}-\mathbf{y}\|^2}u(\mathbf{y})\,\mathrm{d}\sigma_{\mathbf{y}}, \qquad \mathbf{x}\in\Psi.$$

For sake of simplicity, we suppose that $\operatorname{diam} D < 1$ to ensure that $V_{\Phi\Phi}$ is invertible, cf. [24]. Then, the normal derivative of w is given by the Dirichlet-to-Neumann map

$$\begin{bmatrix} V_{\Gamma\Gamma} & V_{\Sigma\Gamma} \\ V_{\Gamma\Sigma} & V_{\Sigma\Sigma}\end{bmatrix}\begin{bmatrix} \frac{\partial w}{\partial \mathbf{n}}\big|_\Gamma \\ \frac{\partial w}{\partial \mathbf{n}}\big|_\Sigma\end{bmatrix} = \begin{bmatrix} \frac12 + K_{\Gamma\Gamma} & K_{\Sigma\Gamma} \\ K_{\Gamma\Sigma} & \frac12 + K_{\Sigma\Sigma}\end{bmatrix}\begin{bmatrix} 0 \\ f\end{bmatrix}, \tag{2.16}$$

cf. (1.7). Likewise, the unknown boundary data of v_i are determined by

$$\begin{bmatrix} V_{\Gamma\Gamma} & -K_{\Sigma\Gamma} \\ -V_{\Gamma\Sigma} & \frac12 + K_{\Sigma\Sigma}\end{bmatrix}\begin{bmatrix} \frac{\partial v}{\partial \mathbf{n}}\big|_\Gamma \\ v|_\Sigma\end{bmatrix} = \begin{bmatrix} \frac12 + K_{\Gamma\Gamma} & -V_{\Sigma\Gamma} \\ -K_{\Gamma\Sigma} & V_{\Sigma\Sigma}\end{bmatrix}\begin{bmatrix} 0 \\ g_i\end{bmatrix}. \tag{2.17}$$

2.2. **Boundary element method.** The shape functional and its gradient can be computed from the knowledge of the boundary data of the state equations (1.7) and (1.10). These data are given by the boundary integral equations (2.16) and (2.17). Hence, it is rather convenient to employ a boundary element method to compute the required boundary data of the state equations. We use a Galerkin discretization by N_Φ piecewise linear functions $\{\theta_i^\Phi\}_{i=1}^{N_\Phi}$ on each boundary $\Phi \in \{\Sigma, \Gamma\}$. For $\Phi, \Psi \in \{\Sigma, \Gamma\}$, we introduce the system matrices

$$\mathbf{V}_{\Phi\Psi} = -\frac{1}{2\pi}\left[\int_\Psi\int_\Phi \log\|\mathbf{x}-\mathbf{y}\|\theta_i^\Phi(\mathbf{y})\theta_j^\Psi(\mathbf{x})\,\mathrm{d}\sigma_{\mathbf{y}}\,\mathrm{d}\sigma_{\mathbf{x}}\right]_{i=1,\dots,N_\Phi,\, j=1,\dots,N_\Psi},$$
$$\mathbf{K}_{\Phi\Psi} = \frac{1}{2\pi}\left[\int_\Psi\int_\Phi \frac{\langle \mathbf{x}-\mathbf{y}, \mathbf{n}_{\mathbf{y}}\rangle}{\|\mathbf{x}-\mathbf{y}\|^2}\theta_i^\Phi(\mathbf{y})\theta_j^\Psi(\mathbf{x})\,\mathrm{d}\sigma_{\mathbf{y}}\,\mathrm{d}\sigma_{\mathbf{x}}\right]_{i=1,\dots,N_\Phi,\, j=1,\dots,N_\Psi},$$

and the mass matrices

$$\mathbf{M}_\Phi = \left[\int_\Phi \theta_i^\Phi(\mathbf{x})\theta_j^\Phi(\mathbf{x})\,\mathrm{d}\sigma_{\mathbf{x}}\right]_{i,j=1,\dots,N_\Phi},$$

and the load vectors of Dirichlet data f_Σ and Neumann data $g_{i,\Sigma}$

$$\mathbf{f}_\Sigma = \left[\int_\Sigma \theta_i^\Sigma(\mathbf{x})f(\mathbf{x})\,\mathrm{d}\sigma_{\mathbf{x}}\right]_{i=1,\dots,N_\Sigma}, \qquad \mathbf{g}_{i,\Sigma} = \left[\int_\Sigma \theta_i^\Sigma(\mathbf{x})g_i(\mathbf{x})\,\mathrm{d}\sigma_{\mathbf{x}}\right]_{i=1,\dots,N_\Sigma}.$$

Then, the linear system of equations

$$\begin{bmatrix} \mathbf{V}_{\Gamma\Gamma} & \mathbf{V}_{\Sigma\Gamma} \\ \mathbf{V}_{\Gamma\Sigma} & \mathbf{V}_{\Sigma\Sigma}\end{bmatrix}\begin{bmatrix} \mathbf{a}_\Gamma \\ \mathbf{a}_\Sigma\end{bmatrix} = \begin{bmatrix} \frac12\mathbf{M}_\Gamma + \mathbf{K}_{\Gamma\Gamma} & \mathbf{K}_{\Sigma\Gamma} \\ \mathbf{K}_{\Gamma\Sigma} & \frac12\mathbf{M}_\Sigma + \mathbf{K}_{\Sigma\Sigma}\end{bmatrix}\begin{bmatrix} \mathbf{0} \\ \mathbf{M}_\Sigma^{-1}\mathbf{f}_\Sigma\end{bmatrix}, \tag{2.18}$$

gives us the Neumann data $(\partial w/\partial \mathbf{n})|_\Gamma \approx \sum_{j=1}^{N_\Gamma}[\mathbf{a}_\Gamma]_j\theta_j^\Gamma$ on Γ and $(\partial w/\partial \mathbf{n})|_\Sigma \approx \sum_{j=1}^{N_\Sigma}[\mathbf{a}_\Sigma]_j\theta_j^\Sigma$ on Σ from the Dirichlet data f on Σ. Likewise, the system

$$\begin{bmatrix} \mathbf{V}_{\Gamma\Gamma} & -\mathbf{K}_{\Sigma\Gamma} \\ -\mathbf{V}_{\Gamma\Sigma} & \frac{1}{2}\mathbf{M}_\Sigma + \mathbf{K}_{\Sigma\Sigma} \end{bmatrix} \begin{bmatrix} \mathbf{b}_\Gamma \\ \mathbf{b}_\Sigma \end{bmatrix} = \begin{bmatrix} \frac{1}{2}\mathbf{M}_\Gamma + \mathbf{K}_{\Gamma\Gamma} & -\mathbf{V}_{\Sigma\Gamma} \\ -\mathbf{K}_{\Gamma\Sigma} & \mathbf{V}_{\Sigma\Sigma} \end{bmatrix} \begin{bmatrix} \mathbf{0} \\ \mathbf{M}_\Sigma^{-1}\mathbf{g}_{i,\Sigma} \end{bmatrix}, \tag{2.19}$$

yields the Dirichlet data $v_i|_\Gamma = \sum_{j=1}^{N_\Gamma}[\mathbf{b}_\Gamma]_j\theta_j^\Gamma$ on Γ and the Neumann data $(\partial v_i/\partial \mathbf{n})|_\Sigma \approx \sum_{j=1}^{N_\Sigma}[\mathbf{b}_\Sigma]_j\theta_j^\Sigma$ on Σ from the given Neumann data $\mathbf{g}_{i,\Sigma}$ on Σ.

We mention that the appearing system matrices have to be computed only once for each domain while the system (2.19) has to be solved $M+1$ times to get the v_i's from the g_i's. We will use the *wavelet Galerkin scheme* which yields quasi sparse system matrices and, hence, a linear overall complexity with respect to the number $N_\Gamma + N_\Sigma$ of degrees of freedom. We refer to [20] for all the details on the wavelet based fast solution of boundary integral equations.

2.3. **Approximation of the free boundary.** For the numerical computations, we restrict ourselves to inclusions which are starshaped with respect to the origin $\mathbf{0}$. Then, the inclusion can be parametrized in accordance with

$$\gamma : [0, 2\pi] \to \Gamma, \qquad \phi \mapsto r(\phi) \begin{bmatrix} \cos\phi \\ \sin\phi \end{bmatrix},$$

i.e., we can identify the inclusion via a radial function

$$r(\phi) = a_0 + \sum_{n=1}^{\infty} a_n \cos(n\phi) + a_{-n}\sin(n\phi) \in C^2_{\mathrm{per}}([0, 2\pi]),$$

which depends only on the polar angle. Hence, it is reasonable to make for the sought inclusion the ansatz

$$r_{N_r}(\phi) = a_0 + \sum_{n=1}^{N_r} a_n \cos(n\phi) + a_{-n}\sin(n\phi). \tag{2.20}$$

Since r_{N_r} admits $2N_r + 1$ degrees of freedom $a_{-N_r}, a_{1-N_r}, \ldots, a_{N_r}$, we arrive at a finite dimensional optimization problem in the open set

$$A_{N_r} := \big\{a_{-N_r}, a_{1-N_r}, \ldots, a_{N_r} \in \mathbb{R} : r_{N_r}(\phi) > 0,\ \phi \in [0, 2\pi]\big\} \subset \mathbb{R}^{2N_r+1}.$$

Hence, via the identification $r_{N_r} \Leftrightarrow D_{N_r}$, the finite dimensional approximation of shape minimization problem (1.2) reads as

$$F(D_{N_r}) \to \min_{A_{N_r}}. \tag{2.21}$$

The associated gradient has to be computed with respect to all directions under consideration:

$$\mathbf{V}(\phi) = \cos(N_r\phi)\mathbf{e}_r(\phi), \cos\big((N_r-1)\phi\big)\mathbf{e}_r(\phi), \ldots, \sin\big((N_r-1)\phi\big)\mathbf{e}_r(\phi), \sin(N_r\phi)\mathbf{e}_r(\phi).$$

Herein, $\mathbf{e}_r(\phi) = (\cos\phi, \sin\phi)$ is the radial direction.

We will apply the quasi-Newton method, updated by the inverse BFGS-rule without damping, in combination with a quadratic line-search in order to solve the minimization problem (2.21). For all the details and a survey on available optimization algorithms, we refer to [15, 16, 19] and the references therein.

3. Numerical results

In our numerical example, we consider D to be the ellipse with semi-axes 0.45 and 0.3, having a starshaped inclusion in its interior. This inclusion is to be determined from measurements of the Neumann data for the single voltage distribution $f(\mathbf{x}) = x_1^2 - x_2^2$ at the outer boundary Σ.

We consider the situation that the noisy measurement $g(\mathbf{x}, \omega)$ is a Gaussian random field. Then, the Neumann data $g(\mathbf{x}, \omega)$ are given in accordance with (1.8), being fully described by having normalized Gaussian random variables $Y_i \sim \mathcal{N}(0, 1)$ and a certain covariance kernel

$$\mathrm{Cor}(\mathbf{x}, \mathbf{y}) = \int_\Omega \big(g(\mathbf{x}, \omega) - g_0(\mathbf{x})\big)\big(g(\mathbf{y}, \omega) - g_0(\mathbf{y})\big)\, \mathrm{d}\mathbb{P}(\omega).$$

We assume for our test that the covariance kernel is a Gaussian kernel

$$\mathrm{Cor}(\mathbf{x}, \mathbf{y}) = \beta \exp\left(- \frac{\|\mathbf{x} - \mathbf{y}\|^2}{\ell^2} \right)$$

with correlation length $\ell > 0$. Hence, by means of the Karhunen-Loève expansion and an appropriate random number generator, we are able to simulate the Gaussian random field numerically, see [18, 27] for example.

The discretization of the shape optimization problem is as follows. The sought inclusion is approximated by a Fourier expansion of with 33 Fourier coefficients, i.e., it holds $N_r = 16$ in (2.20). Notice that the sought inclusion cannot be exactly represented by this Fourier expansion. Moreover, the solutions of the boundary integral equations (2.16) and (2.17) are approximately computed by using 512 piecewise linear wavelets per boundary. We use always the circle of radius 0.2 as initial guess and stop the quasi-Newton method after 25 steps since the underlying shape identification problem is severely ill-posed.

3.1. **Classical approach.** The classical approach would be to sample the process g and to minimize the Kohn-Vogelius functional for each realization. In Figure 3.2, we plotted ten reconstructions which were derived from a single measurement, where the correlation length is set to $\ell = 0.1$ and the noise level β is chosen such that the perturbation $\|g(\omega) - g_0\|_{L^2(\Sigma)}$ is about 5 percent of $\|g_0\|_{L^2(\Sigma)}$. We observe a great variance of the reconstructions in Figure 3.2. In particular, the reconstructions differ mostly considerably from the exact inclusion, which is indicated in dark gray.

Since we are using a parametrization (2.20) based on Fourier coefficients, we can compute the mean of the Fourier coefficients of the reconstructions. Doing so for the ten reconstructions found

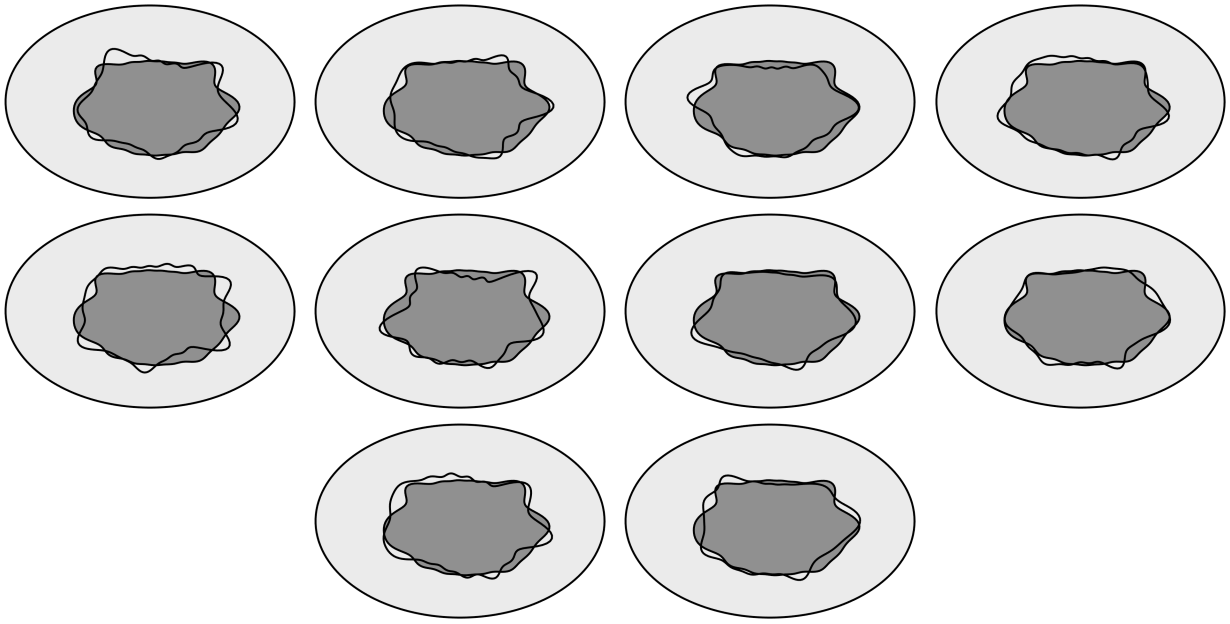

FIGURE 3.2. Reconstructions for ten different realizations of the noisy data.

in Figure 3.2, we obtain the inclusion seen in Figure 3.3. One clearly observes an improvement of the reconstruction. Nonetheless, this parametrization based notion of the mean shape is not generally possible. In particular, it is computationally extremely expensive.

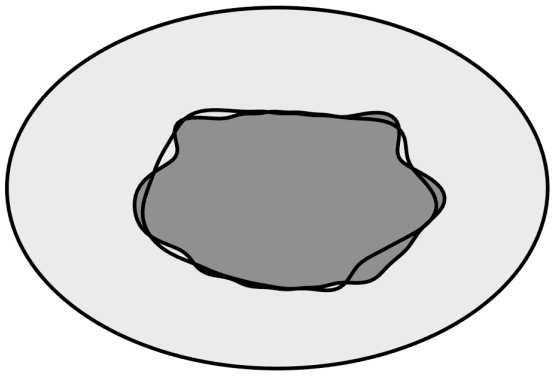

FIGURE 3.3. Mean of the reconstructed inclusions.

3.2. **Expected Kohn-Vogelius functional.** To realize the new approach proposed on this article, we repeat the measurement M times, yielding samples $g^{(1)}, g^{(2)}, \ldots, g^{(M)}$ of the unknown

random field $g(\omega)$. From these measurements, we compute the sample mean

$$\overline{g}(\mathbf{x}) = \frac{1}{M} \sum_{m=1}^{M} g^{(m)}(\mathbf{x})$$

to approximate the mean g_0 in (1.8). The random variation is approximated by means of the Karhunen-Loève expansion with respect to the sample covariance

$$Q(\mathbf{x}, \mathbf{y}) = \frac{1}{M-1} \sum_{m=1}^{M} g^{(m)}(\mathbf{x}) g^{(m)}(\mathbf{y}).$$

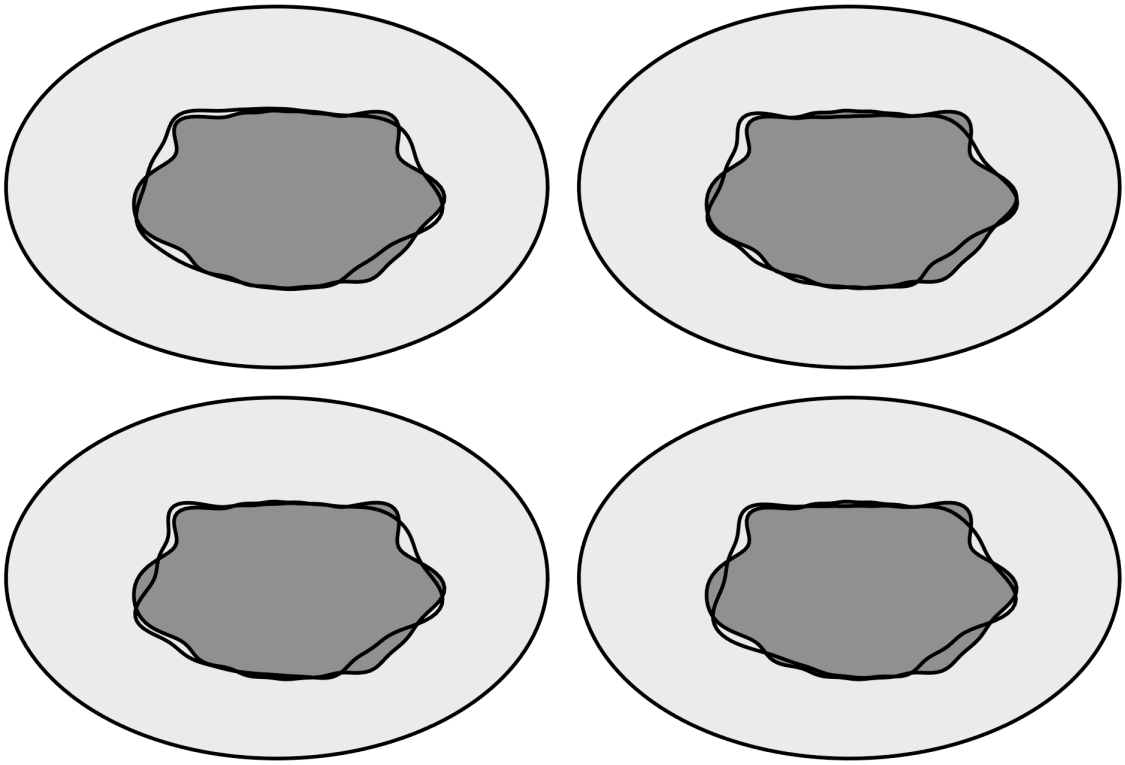

FIGURE 3.4. Reconstructions for the expected Kohn-Vogelius functional in case of 10 samples.

If we run the optimization for the expected Kohn-Vogelius functional, i.e., for the objective (1.5) with $\alpha = 0$, then we obtain the reconstructions found Figure 3.4. Here, we have repeated the reconstruction algorithm four times based on $M = 10$ samples each. One observes much better reconstructions than those which are obtained from a single measurement. Nonetheless, there is still a slight deviation of the reconstructions. This stems from the fact that ten samples are not sufficient to reliably estimate the expectation and the covariance. The situation changes if we exploit 100 measurements. In this case, we obtain a slightly improved reconstruction, see Figure 3.5. Especially, there is no more difference when repeating the experiment.

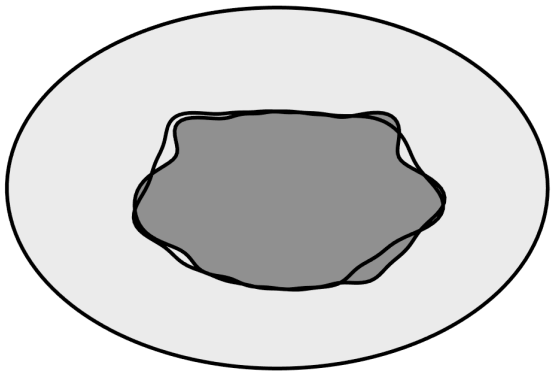

FIGURE 3.5. Reconstruction for the expected Kohn-Vogelius functional in case of 100 samples.

3.3. **Influence of the coupling parameter α.** So far, we only considered the minimization of the expected Kohn-Vogelius functional, which means the particular choice $\alpha = 0$ in the objective (1.4) and (1.5), respectively. Therefore, we shall study the dependence of the reconstruction algorithm on the coupling parameter α. To that end, we choose $M = 100$ samples in order to ensure that the reconstruction does not depend on the particular samples.

We consider objective (1.5), since the standard deviation exhibits the same scaling as the expectation. For our test example, both quantities have a similar size for the initial shape. For increasing coupling parameter α, the standard deviation of the Kohn-Vogelius functional becomes more and more important compared with its expectation. Nonetheless, the reconstruction is basically the same as seen in Figure 3.6. Here, one finds the reconstructions for $\alpha = 1/2$, $\alpha = 3/4$, $\alpha = 7/8$, and $\alpha = 15/16$.

What differs for different values of the coupling parameter α is the convergence behaviour of the reconstruction algorithm. Increasing α enforces faster convergence in the beginning of the minimization algorithm, see also Figure 3.7, where the convergence histories of the objective (1.5) are found for different values of the coupling parameter α. Nonetheless, one also figures out that the functional becomes more flat as α increases. Notice that the reconstruction algorithm does not converge anymore for values of α higher than $\alpha = 15/16$.

4. Conclusion

In the present article, we have proposed a method which enables to reconstruct inclusions or void in electrical impedance tomography also in case of very noisy data. Namely, we modeled the measurement data as random field which can approximately be determined from repeated measurements. An objective which combines the expectation and variance of the Kohn-Vogelius functional is then mimimized to reconstruct the sought inclusion. In particular, it is shown that

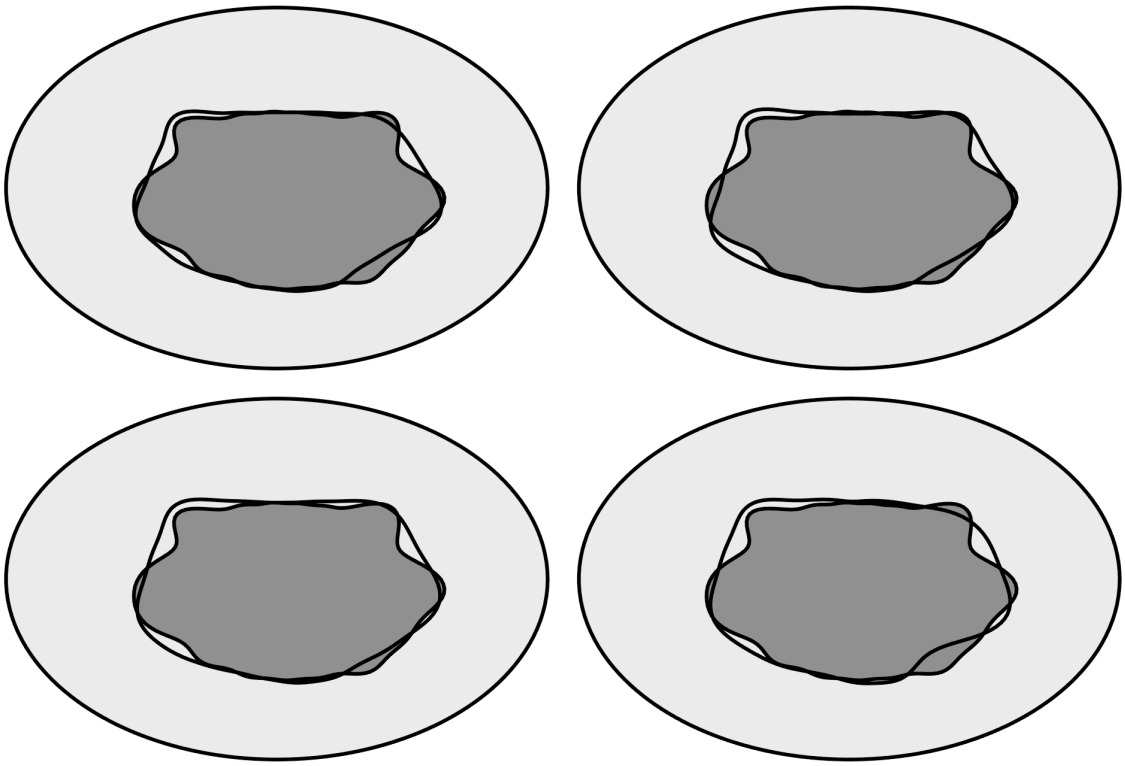

FIGURE 3.6. Influence of the coupling parameter: $\alpha = 1/2, 3/4, 7/8, 15/16$ (from the top to the bottom and from the the left to the right).

the objective as well as its shape gradient is a deterministic quantity. Numerical results are present which show the capability and feasibility of the proposed approach.

REFERENCES

[1] L. Afraites, M. Dambrine, and D. Kateb. Conformal mapping and inverse conductivity problem with one measurement. *ESAIM Control Optim. Calc. Var.*, 13(1):163–177, 2007.

[2] L. Afraites, M. Dambrine, and D. Kateb. Shape methods for the transmission problem with a single measurement. *Numer. Funct. Anal. Optim.*, 28(5–6):519–551, 2007.

[3] L. Afraites, M. Dambrine, and D. Kateb. On second order shape optimization methods for electrical impedance tomography. *SIAM J. Control Optim.*, 47(3):1556–1590, 2008.

[4] I. Akduman and R. Kress. Electrostatic imaging via conformal mapping. *Inverse Problems*, 18:1659–1672, 2002.

[5] G. Alessandrini, V. Isakov, and J. Powell. Local uniqueness in the inverse problem with one measurement. *Trans. Am. Math. Soc.*, 347:3031–3041, 1995.

[6] M. Badra, F. Caubet, and M. Dambrine. Detecting an obstacle immersed in a fluid by shape optimization methods. *Math. Models Methods Appl. Sci.*, 21(10):2069–2101, 2011.

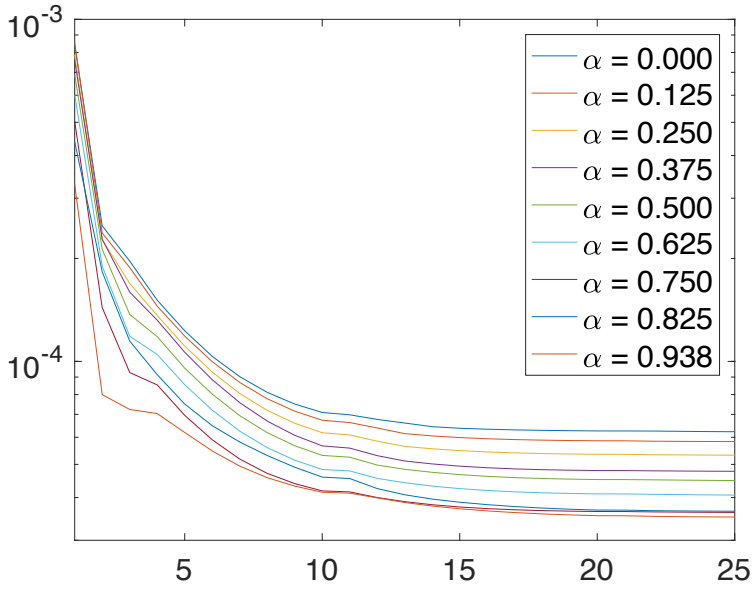

FIGURE 3.7. Convergence histories of the objective for different choices of α.

[7] M. Brühl. Explicit characterization of inclusions in electrical impedance tomography. SIAM J. Math. Anal., 32(6):1327–1341, 2001.

[8] M. Brühl and M. Hanke. Numerical implementation of two noniterative methods for locating inclusions by impedance tomography. Inverse Problems, 16(4):1029–1042, 2000.

[9] R. Chapko and R. Kress. A hybrid method for inverse boundary value problems in potential theory, 2003. *J. Inv. Ill-Posed Problems*, 13(1):27–40, 2005.

[10] M. Dambrine, C. Dapogny, and H. Harbrecht. Shape optimization for quadratic functionals and states with random right-hand sides. *SIAM J. Control Optim.*, 53(5):3081–3103, 2015.

[11] M. Dambrine, H. Harbrecht, M. Peters, and B. Puig. On Bernoulli's free boundary problem with a random boundary. *Int. J. Uncertain. Quantif.*, 7(4):335–353, 2017.

[12] M. Delfour and J.-P. Zolesio. *Shapes and Geometries*. SIAM, Philadelphia, 2001.

[13] K. Eppler and H. Harbrecht. A regularized Newton method in electrical impedance tomography using shape Hessian information. *Control Cybernet.*, 34:203–225, 2005.

[14] K. Eppler and H. Harbrecht. Shape optimization for 3D electrical impedance tomography. In R. Glowinski and J. Zolesio, editors, *Free and Moving Boundaries: Analysis, Simulation and Control*, volume 252 of *Lecture Notes in Pure and Applied Mathematics*, pages 165–184, Chapman & Hall/CRC, Boca Raton, FL, 2007.

[15] A.V. Fiacco and G.P. McCormick. *Nonlinear Programming: Sequential Unconstrained Minimization Techniques*. Wiley, New York, 1968.

[16] R. Fletcher. *Practical Methods for Optimization*. Wiley, New York, 1980.

[17] A. Friedman and V. Isakov. On the uniqueness in the inverse conductivity problem with one measurement. *Indiana Univ. Math. J.*, 38:563–579, 1989.

[18] R. Ghanem and P. Spanos. *Stochastic Finite Elements. A Spectral Approach*. Springer, New York, 1991.

[19] C. Grossmann and J. Terno. *Numerik der Optimierung*. B.G. Teubner, Stuttgart, 1993.

[20] H. Harbrecht and R. Schneider. Wavelet Galerkin schemes for 2D-BEM. In J. Elschner et al., editors, *Problems and Methods in Mathematical Physics (Chemnitz, 1999)*, volume 121 of *Operator Theory: Advances and Applications*, pages 221–260, Birkhäuser, Basel, 2001.

[21] F. Hettlich and W. Rundell. The determination of a discontinuity in a conductivity from a single boundary measurement. *Inverse Problems*, 14:67–82, 1998.

[22] A. Henrot and M. Pierre. *Shape Variation and Optimization*. Tracts in Mathematics 28, European Mathematical Society, 2017.

[23] W. Lionheart, N. Polydorides, and A. Borsic. Electrical Impedance Tomography: Methods, History and Applications. In D.S. Holder, editor, *IOP Series in Medical Physics and Biomedical Engineering*, pages 3–64, Institute of Physics Publishing, 2005.

[24] G. Hsiao and W. Wendland. A finite element method for some equations of first kind. *J. Math. Anal. Appl.*, 58:449–481, 1977.

[25] R. Kress. Inverse Dirichlet problem and conformal mapping. *Math. Comp. Simulation*, 66:255–265, 2004.

[26] R. Kohn and M. Vogelius. Determining conductivity by boundary measurements. *Comm. Pure Appl. Math.*, 37:289–298, 1984.

[27] M. Loève. *Probability theory. I+II*. Fourth edn., volume 45 of *Graduate Texts in Mathematics*, Springer, New York, 1977.

[28] O. Pironneau. *Optimal Shape Design for Elliptic Systems*. Springer, New York, 1984.

[29] J.-R. Roche and J. Sokolowski. Numerical methods for shape identification problems. *Control Cybern.* 25:867–894, 1996.

[30] J. Sokolowski and J.-P. Zolesio. *Introduction to Shape Optimization*. Springer, Berlin, 1992.

Marc Dambrine and Benedicte Puig, CNRS / Univ Pau & Pays Adour, Laboratoire de Mathématiques et de leurs Applications de Pau - Fédération IPRA, UMR 5142, 64000, Pau, France.

E-mail address: {marc.dambrine,benedicte.puig}@univ-pau.fr

Departement für Mathematik und Informatik, Universität Basel, Spiegelgasse 1, 4051 Basel, Switzerland.

E-mail address: helmut.harbrecht@unibas.ch

LATEST PREPRINTS

No.	Author: *Title*
2016-24	**F. Amoroso, D. Masser** *Lower bounds for the height in Galois extensions*
2016-25	**W. D. Brownawell, D. W. Masser** *Zero estimates with moving targets*
2016-26	**H. Derksen, D. Masser** *Linear equations over multiplicative groups, recurrences, and mixing III*
2016-27	**D. Bertrand, D. Masser, A. Pillay, U. Zannier** *Relative Manin-Mumford for semi-abelian surfaces*
2016-28	**L. Capuano, D. Masser, J. Pila, U. Zannier** *Rational points on Grassmannians and unlikely intersections in tori*
2016-29	**C. Nobili, F. Otto** *Limitations of the background field method applied to Rayleigh-Bénard convection*
2016-30	**W. D. Brownawell, D. W. Masser** *Unlikely intersections for curves in additive groups over positive characteristic*
2016-31	**M. Dambrine, H. Harbrecht, M. D. Peters, B. Puig** *On Bernoulli's free boundary problem with a random boundary*
2016-32	**H. Harbrecht, J. Tausch** *A fast sparse grid based space-time boundary element method for the nonstationary heat equation*
2016-33	**S. Iula** *A note on the Moser-Trudinger inequality in Sobolev-Slobodeckij spaces in dimension one*
2016-34	**C. Bürli, H. Harbrecht, P. Odermatt, S. Sayasone, N. Chitnis** *Mathematical analysis of the transmission dynamics of the liver fluke, Opisthorchis viverrini*
2017-01	**J. Dölz and T. Gerig, M. Lüthi, H. Harbrecht and T. Vetter** *Efficient computation of low-rank Gaussian process models for surface and image registration*
2017-02	**M. J. Grote, M. Mehlin, S. A. Sauter** *Convergence analysis of energy conserving explicit local time-stepping methods for the wave equation*

Preprints are available under *https://math.unibas.ch/research/publications*

LATEST PREPRINTS

No.	Author: *Title*
2017-03	**Y. Bilu, F. Luca, D. Masser** *Collinear CM-points*
2017-04	**P. Zaspel** *Ensemble Kalman filters for reliability estimation in perfusion inference*
2017-05	**J. Dölz and H. Harbrecht** *Hierarchical Matrix Approximation for the Uncertainty Quantification of Potentials on Random Domains*
2017-06	**P. Zaspel** *Analysis and parallelization strategies for Ruge-Stüben AMG on many-core processors*
2017-07	**H. Harbrecht and M. Schmidlin** *Multilevel Methods for Uncertainty Quantification of Elliptic PDEs with Random Anisotropic Diffusion*
2017-08	**M. Griebel and H. Harbrecht** *Singular value decomposition versus sparse grids: Refined complexity Estimates*
2017-09	**J. Garcke and I. Kalmykov** *Efficient Higher Order Time Discretization Schemes for Hamilton-Jacobi-Bellman Equations Based on Diagonally Implicit Symplectic Runge-Kutta Methods*
2017-10	**M. J. Grote and U. Nahum** *Adaptive Eigenspace Regularization For Inverse Scattering Problems*
2017-11	**J. Dölz, H. Harbrecht, S. Kurz, S. Schöps and F. Wolf** *A Fast Isogeometric BEM for the Three Dimensional Laplace- and Helmholtz Problems*
2017-12	**P. Zaspel** *Algorithmic patterns for $\mathcal{H}$-matrices on many-core processors*
2017-13	**R. Brügger, R. Croce and H. Harbrecht** *Solving a free boundary problem with non-constant coefficients*
2017-14	**M. Dambrine, H. Harbrecht and B. Puig** *Incorporating knowledge on the measurement noise in electrical impedance tomography*

Preprints are available under *https://math.unibas.ch/research/publications*